Correcting the FRA Systematic Error in VTEC Maps from SMOS Radiometric Data

Journal:	*Transactions on Geoscience and Remote Sensing*
Manuscript ID	TGRS-2022-00682.R1
Manuscript Type:	Regular paper
Date Submitted by the Author:	n/a
Complete List of Authors:	Rubino, Roselena; Universitat Politecnica de Catalunya, Signal Theory and Communications Department Duffo, Nuria; Universitat Politècnica de Catalunya, Dept of Signal Theory and Communications; González, Verónica; Consejo Superior de Investigaciones Científicas, Oceanografía Física y Tecnológica Corbella, Ignasi; Universitat Politecnica de Catalunya, Signal Theory and Communications; Torres, Francesc; Universitat Politècnica de Catalunya, Signal Theory and Communications Oliva, Roger; European Space Agency, ESAC MARTIN-NEIRA, Manuel; European Space Agency, TEC-EF
Keywords:	Electromagnetics for Remote Sensing, Microwave Radiometry, Atmosphere, Oceans and Water

DOI 10.1109/TGRS.2022.3215111

Correcting the FRA Systematic Error in VTEC Maps from SMOS Radiometric Data

Roselena Rubino, Nuria Duffo, *Senior Member, IEEE*, Verónica González-Gambau, *Member, IEEE*, Ignasi Corbella, Francesc Torres, *Senior Member, IEEE*, Roger Oliva, *Member, IEEE*, and Manuel Martín-Neira, *Senior Member, IEEE*

***Abstract*—The Faraday Rotation (FR) is a non-negligible effect at the L-band, which is the operation frequency of the Soil Moisture and Ocean Salinity (SMOS) mission. This effect introduces a rotation in the electromagnetic field polarization when propagating through the ionosphere that must be compensated. Recently, a methodology was developed in order to retrieve the Vertical Total Electron Content (VTEC) from SMOS radiometric data with the aim to better correct the Faraday rotation effect [1]. In that work, systematic patterns in the retrieved Faraday Rotation Angle (FRA) were detected. In this paper, these systematic patterns are characterized and corrected to improve the quality of the retrieved VTEC maps. These maps can be then re-used in the SMOS level 2 processor for the correction of the FRA in the mission. The impact of using the SMOS-derived VTEC maps instead of the VTEC data from GPS measurements on the ocean brightness temperature measurement has also been analyzed. Results of this analysis show that the usage of those maps allows a significant enhancement in the quality of the brightness temperatures, which will lead to an improvement on salinity retrievals.**

***Index Terms*—Faraday Rotation Angle (FRA), Soil Moisture and Ocean Salinity (SMOS), Vertical Total Electron Content (VTEC)**

I. Introduction

WHEN the microwave radiation from Earth propagates through the ionosphere and it is measured from space, its electromagnetic field components are rotated a certain angle due to a physical phenomenon called Faraday rotation (FR). Such is the case in the Soil Moisture and Ocean Salinity (SMOS) mission when its payload Microwave Imaging Radiometer Aperture Synthesis (MIRAS) measures the polarimetric Brightness Temperatures (TB) coming from the Earth's Surface.

The Faraday Rotation Angle (FRA) in the polarization of an electromagnetic field depends on different variables as expressed in equation (1) [2], [3]:

$$\Omega_f = 1.355 * 10^4 f^{-2} B_0 \cos\Theta_B \sec\theta * VTEC \quad (1)$$

where Ω_f represents the FRA in degrees; f, the frequency in GHz (1.4135 GHz in SMOS); B_0, the Geomagnetic Field in Teslas; Θ_B, the angle between the magnetic field and the wave propagation direction; θ, the incidence angle; and $VTEC$, the Vertical Total Electron Content in TEC Units (TECU) [10^{16} $electrons/m^2$]. Both the Geomagnetic Field and the VTEC are given at a geodetic altitude of 450 km. In order to compensate the FRA, data provided by external sources can be used in the classical formulation (1): the Geomagnetic Field from the International Geomagnetic Reference Field (IGRF) [4] and the so called "consolidated TEC" (hereafter, L1 VTEC) provided by the SMOS Data Processing Ground Segment (DPGS) [5].

The FRA can also be retrieved from full polarimetric radiometric data in an instantaneous way –called from now on estimated measured FRA (Ω_f^m)– as it is expressed in (2) [6], where φ corresponds to the geometrical rotation angle (specific to the platform's attitude and instrument orientation), and the terms T_B^{xx}, T_B^{yy}, and T_B^{xy}, to the SMOS full-pol brightness temperatures.

$$\Omega_f^m = -\varphi - \frac{1}{2} arctan\left(\frac{2\Re e\left(T_B^{xy}\right)}{T_B^{xx} - T_B^{yy}}\right) \quad (2)$$

However, estimating Faraday rotation out of SMOS radiometric data is not as straightforward as it may seem. MIRAS has relatively poor radiometric sensitivity (thermal noise) and accuracy (spatial bias), which hampers the FRA retrieval with the required accuracy.

In [1], a methodology was presented to allow estimating the

This research was supported by the European Space Agency and Deimos Engenharia (Portugal), SMOS P7 Subcontract DME CP12 no. 2015-005; ERDF (European Regional Development Fund); by the Spanish public funds, projects TEC2017-88850-R and ESP2015-67549-C3-1-R; and through the award "Unidad de Excelencia María de Maeztu" MDM-2016-0600, financed by the "Agencia Estatal de Investigación" (Spain) and by the European Regional Development (ERDF).

R. Rubino, N. Duffo, I. Corbella, and F. Torres are with the CommSensLab Research Group, Polytechnic University of Catalonia, c/Jordi Girona 1-3, 08034 Barcelona, Spain; (e-mail: roselena.rubino@upc.edu, duffo@upc.edu, corbella@upc.edu, francesc.torres@upc.edu).

V. González-Gambau is with the Department of Physical Oceanography, Institute of Marine Sciences, CSIC and Barcelona Expert Center, Passeig Maritim de la Barceloneta, 37-49, 08003 Barcelona, Spain (e-mail: vgonzalez@icm.csic.es).

R. Oliva is with the Zenithal Blue Technologies S.L.U. for the European Space Agency, 08023 Barcelona, Spain (e-mail: roger.oliva.balague@esa.int).

M. Martín-Neira is with the European Space Research and Technology Center, European Space Agency, 2200 AG Noordwijk, The Netherlands (e-mail: manuel.martin-neira@esa.int)

total electron content of the ionosphere from the calculated Faraday rotation angle with the measured SMOS TB. This led to the possibility of retrieving VTEC from the SMOS radiometric data not using models nor VTEC external data sets. This SMOS-derived VTEC product can then be used in the SMOS level 2 processor to correct the Faraday rotation in order to improve the quality of the geophysical retrievals.

However, when analyzing the recoveries, a systematic FRA error pattern was identified. This work characterizes this error and proposes a technique to compensate for it leading to a better accuracy in the VTEC retrievals.

II. Characterization of the FRA Systematic Error

The methodology developed in [1] allows recovering VTEC global maps from full-polarimetric SMOS radiometric data (hereafter, SMOS VTEC) by applying spatial and temporal filtering techniques. Fig. 1 shows VTEC maps: (a) the L1 VTEC (used as a reference), (b) the SMOS-derived VTEC, and (c) the difference between the L1 VTEC and the SMOS-derived. It can be seen that there is an unexpected systematic error pattern affecting the cross-track VTEC geophysical variability.

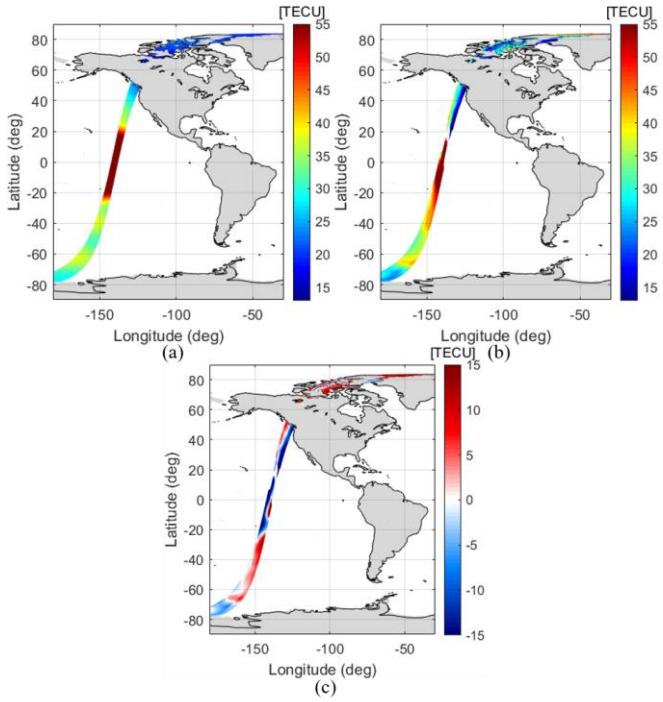

Fig. 1. Descending orbit in March 2014: (a) L1 VTEC, (b) SMOS VTEC, and (c) difference between the SMOS VTEC and the L1 VTEC.

These results suggest that the estimated measured FRA (2) is the sum of the actual FRA (Ω_f) plus a systematic error Δ.

$$\Omega_f^m = \Omega_f + \Delta \quad (3)$$

Orbits where the FRA should tend to zero have been used in order to retrieve the FRA systematic error (Δ term). Fig. 2 shows a Hovmöller plot (time in the x-axis, boresight latitude in the y-axis, average of all the longitudes) of the FRA for all the ascending orbits over the Pacific Ocean from the beginning of the mission until 2021 computed from L1 VTEC. Ascending overpasses are used because the FRA is much lower in the morning (ascending SMOS overpasses are at 6 a.m.) than in the afternoon (descending ones are at 6 p.m.). It can be seen that the FRA tends to 0 around 20°S. In general, values are even lower for the summer months.

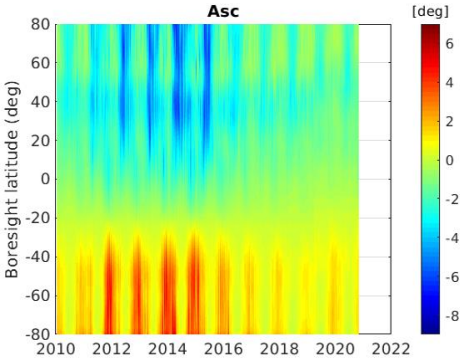

Fig. 2. FRA Hovmöller of ascending orbits.

As a first step, 2017 has been used to calculate Δ because the solar activity is low [7] and as a consequence, also the FRA. Both the geomagnetic rotation angle φ and all brightness temperatures per polarization of three consecutive days of July have been averaged in the latitude range [30°S 5°S] in order to calculate Ω_f^m using Eq. (2). The error term Δ per each point in the snapshot is obtained by subtracting $\Omega_f^m - \Omega_f$ where Ω_f uses (1) with the L1 VTEC as reference. Finally, a spatial filter in the director cosine plane (see [1] for more details on this filter) is applied in order to mitigate the effect of noise in the Δ computation. The resulting FRA systematic error pattern is shown Fig. 3a.

The FRA systematic error has been also computed for years 2018 and 2014 to assess whether Δ can be considered stable in time despite the variation of the solar activity. Fig. 3b and Fig. 3c show both results. Fig. 3d shows the Δ pattern computed by using three consecutive days (15th to 17th of July) per each year in the period 2010-2019. Patterns found from different years are in agreement, corroborating that Δ remains temporally stable. From this analysis, it has been decided to use the same Δ (Fig. 3d) in the FRA correction for the entire mission.

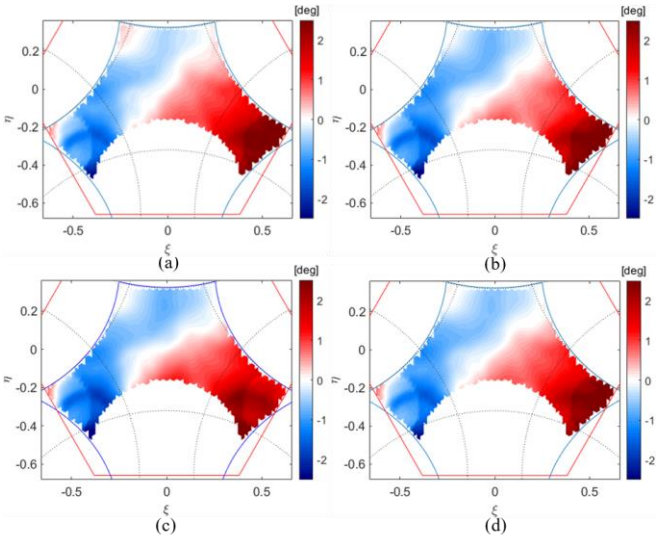

Fig. 3. FRA systematic error in the snapshot (Δ term) computed by using different periods: (a) 2017, (b) 2018, (c) 2014, and (d) from 2010-2019

III. Correcting the Systematic Error

The correction of the FRA systematic error is applied to each one of the FRA snapshots retrieved from the full-polarimetric TB, previous to the computation of the VTEC per snapshot (between steps 2 and 3 of the methodology defined in [1]).

A modification with respect to the methodology proposed in [1] has been introduced. It has been done in the filter that rejects those pixels affected by the indetermination of Eq. (1) when solving for VTEC (the threshold is set to $\cos\Theta_B = 0.05$). This makes possible the recovery in the entire orbit, avoiding gaps in the VTEC maps.

IV. SMOS-derived VTEC maps

Correcting for the FRA systematic error leads to a very significant improvement in the VTEC maps. **¡Error! No se encuentra el origen de la referencia.** shows VTEC maps: (a) the SMOS VTEC retrieved with the refined methodology that includes the correction of the FRA systematic error, (b) the difference between (a) and the L1 VTEC, and (c) the difference between (a) and the recovery without correcting Δ –Fig. 1b–.

As it can be seen, this correction makes possible a VTEC recovery with a variation in the longitudinal axis of the swath more geophysically consistent.

Fig. 5a shows the retrieved VTEC for all the descending orbits in a day (March 20th, 2014, the year with highest solar activity along the mission) after eliminating the FRA systematic error contribution; Fig. 5b, the comparison of the recovery when correcting Δ with respect to the L1 VTEC; and Fig. 5c, the comparison of the recovery when correcting the FRA systematic error contribution and when not doing it. When analyzing Fig. 5b, it can be seen that the recovery does not present any specific pattern across-track with respect to the L1 VTEC.

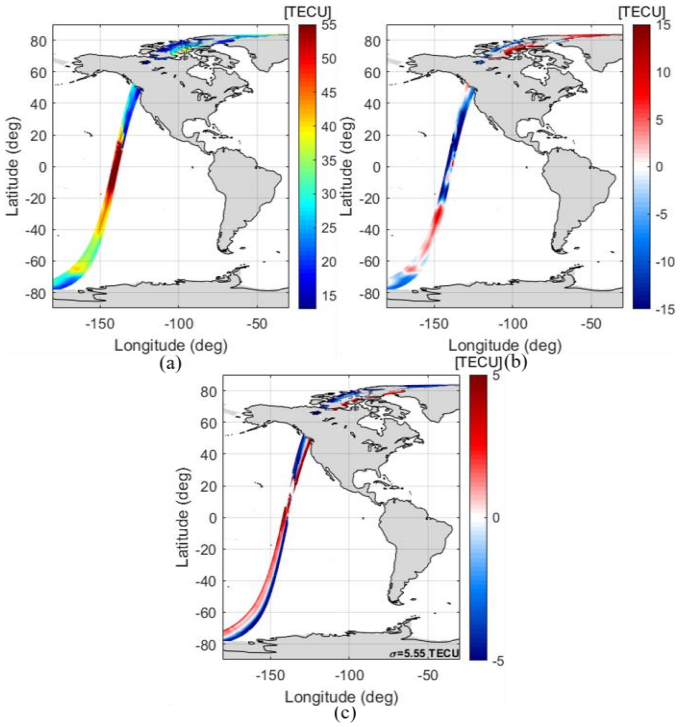

Fig. 4. Descending orbit on March 2014: (a) the SMOS VTEC using the methodology that corrects for the FRA systematic error, (b) the difference of it with respect to the L1 VTEC, and (c) difference between the recovery using the methodology that corrects for the FRA systematic error and the one that does not correct it (Fig. 1b).

V. Impact on Measurements over the Ocean

The recovered VTEC maps can be used in the SMOS Level-2 processor to correct the Faraday rotation and improve the geophysical retrievals.

To analyze the impact of using these VTEC maps on the spatial biases, the difference between the SMOS measured TB and the modeled TB as a function of the spatial direction is computed. The modeled TB has been derived from the Geophysical Model Function (GMF) presented in [8], using geophysical priors for SSS (climatology), SST and wind speed (data provided by ECMWF) [9]. The temporal median of this difference is calculated over a stable region over the South Pacific [10]. In particular, Fig. 6 shows the temporal standard deviation of the difference between SMOS and modeled TB normalized by the radiometric accuracy, which should be close to 1. Fig. 6a shows the metric for the X-polarization when L1 VTEC products are used to generate modeled TB at antenna reference frame, and the Fig. 6b, when the SMOS-derived VTEC maps are used. Fig. 6c and Fig. 6d correspond to the Y-polarization when using the L1 VTEC and the SMOS VTEC, respectively.

From Fig. 6 it is noteworthy that there is a significant improvement in the region of the field of view with high incidence angles (top part of the snapshot) since it is the area where the sensitivity of TB to TEC is higher. The impact of this improved stability is expected to be quite significant in terms of retrieved salinity.

The next step in the assessment has been the analysis of the impact of using the SMOS-derived VTEC maps to correct the FRA instead of the L1 VTEC products on the TB stability. In

order to analyze the stability using both VTEC maps, Hovmöller diagrams of the difference between the SMOS and the modeled TBs per each polarization at antenna reference frame (for the period 2014-2016 by using orbits over the Pacific Ocean) have been generated, which is a usual metric in the SMOS Level 1 Expert Support Laboratories (ESL) for this kind of assessment. The color represents the bias in TB with respect to the model (averaged in the Alias-Free Field of View (AF-FoV)). The y-axis corresponds to the boresight latitude at which the TB measurement has been acquired (using bins of 0.25º of latitude). Fig. 7 and Fig. 8 show the bias in the third Stokes parameter (hereafter, T3) for ascending and descending orbits, respectively. As it was also reported in [11], a strong latitudinal gradient in T3 is found when using the L1 VTEC for correcting the FRA (top plots of Fig. 7 and Fig. 8). As evidenced in these Hovmöllers, the latitudinal gradient in T3 has been substantially mitigated when using the SMOS-derived VTEC maps (bottom plots of Fig. 7 and Fig. 8), improving the stability with respect to the usage of L1 VTEC products (Fig. 7 and Fig. 8, top).

The stability of TB in X and Y-polarizations has also been improved for descending orbits when using SMOS-derived VTEC maps, although the impact is lower than in the bias of T3. Some examples of the difference between the SMOS and modeled TB for X-polarization along descending orbits are shown in Fig. 9 for different dates. The impact is clearly much higher in the southern latitudes, where the sensitivity of TB to TEC is also higher (see Fig. 3a in [12]) and in particular, around 20°S, where there is a pool of high VTEC values (see Fig. 5). Similar results have been obtained for Y-polarization (not shown). In the northern latitudes of these plots, the sensitivity is lower (between 10°N-30°N). In the case of ascending orbits, the impact of using one or the other VTEC product on TB in X and Y-polarizations is really low, which is expected due to the low VTEC values in ascending orbits as compared to descending one.

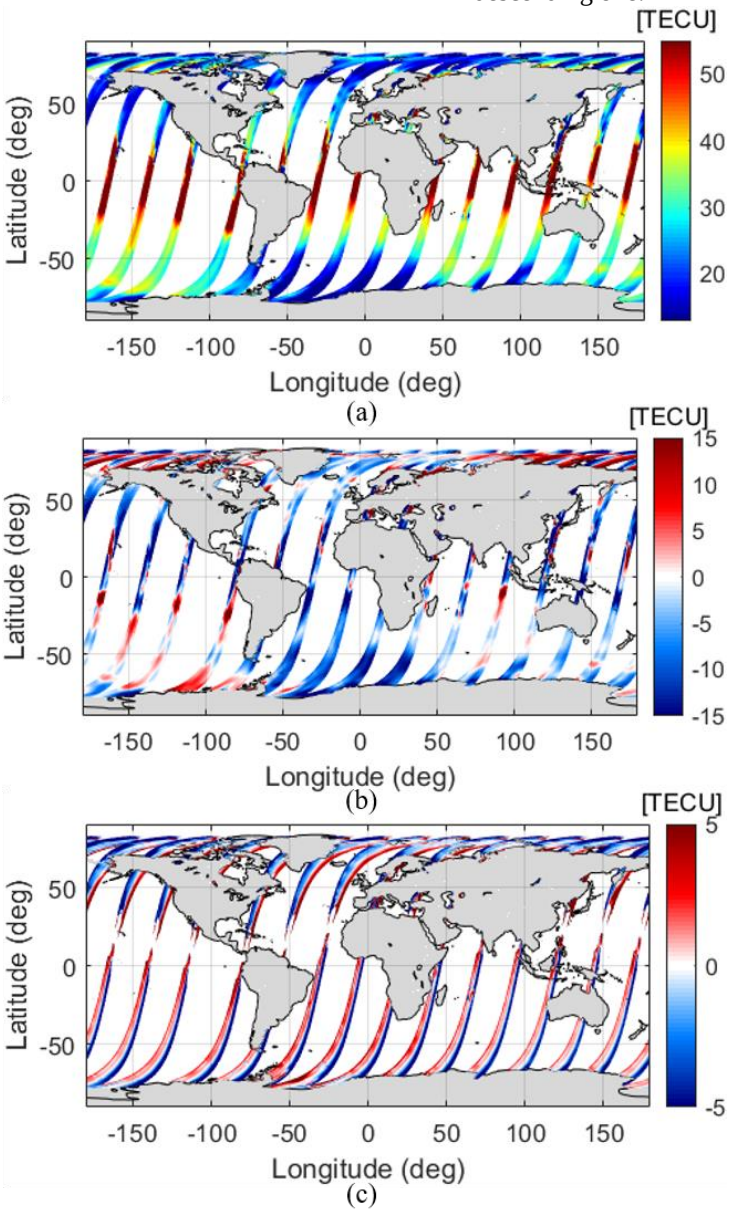

Fig. 5. VTEC of March 20th, 2014: (a) the SMOS VTEC using the methodology that includes the correction of Δ, (b) difference between (a) and the L1 VTEC, and (c) difference between the VTEC recovery when applying the correction of Δ and when not doing it.

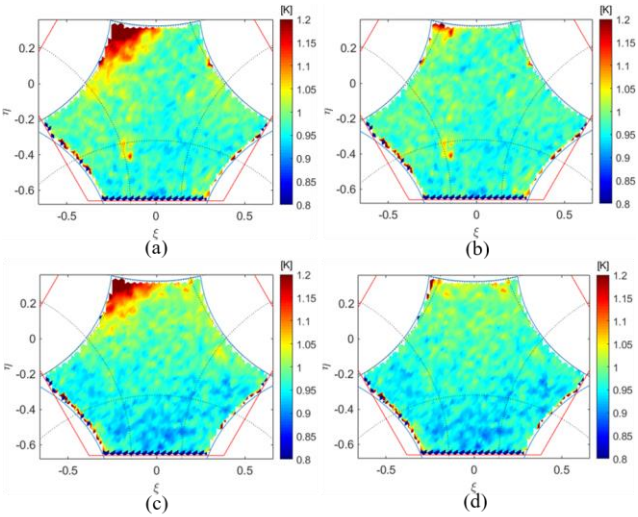

Fig. 6. Standard deviation of the difference between SMOS and modeled TB normalized by the radiometric accuracy: (a) X-pol, when the L1 VTEC is used to transform modeled TB at ocean surface to antenna reference frame, (b) X-pol when the SMOS VTEC is used, (c) Y-pol when the L1 VTEC is used, (d) Y-pol when the SMOS VTEC is used.

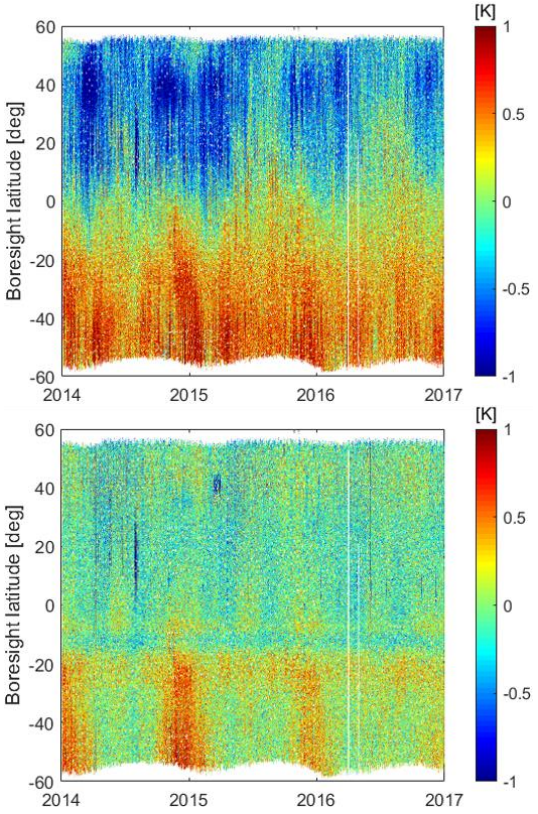

Fig. 7. Hovmöller diagrams of the difference between the SMOS TB and the modeled TB (averaged in the AF-FoV) for the third Stokes parameter at antenna reference frame for ascending orbits. Top: L1 VTEC products have been used to correct for the FR in the modeled TB; bottom: SMOS-derived VTEC maps have been used for the FR correction.

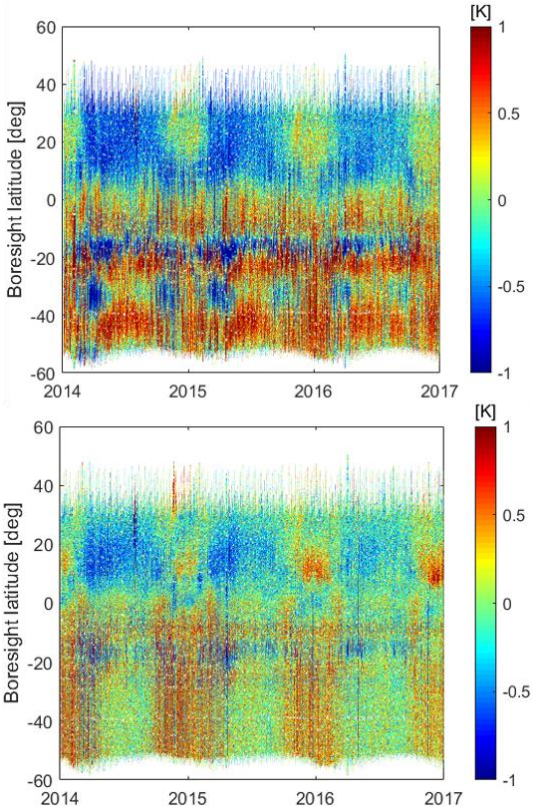

Fig. 8. Hovmöller diagrams of the difference between the SMOS TB and the modeled TB (averaged in the AF-FoV) for the third Stokes parameter at antenna reference frame for descending orbits. Top: L1 VTEC products have been used to correct for the FR in the modeled TB; bottom: SMOS-derived VTEC maps have been used for the FR correction.

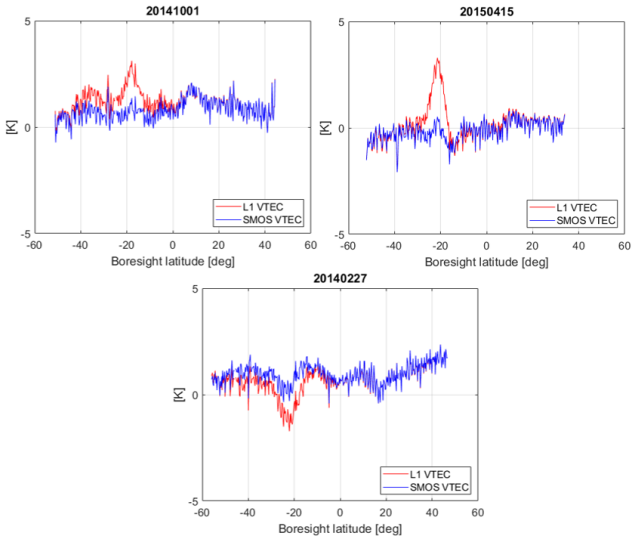

Fig. 9. TB bias with respect to the model in the X-polarization along descending orbits for several dates.

Finally, the impact has been analyzed on daily global maps of the ocean TB anomaly (defined as the difference between SMOS TB once corrected for spatial biases [10] and the theoretically modeled TB). This is the magnitude that enters in the sea surface salinity (SSS) retrieval scheme in order to calculate it. Therefore, it is a quality indicator for the SSS retrievals. Fig. 10 shows a daily descending map for X-polarization. Note that the maps do not cover the southern high latitudes, mainly due to the sea-ice cover (Austral winter).

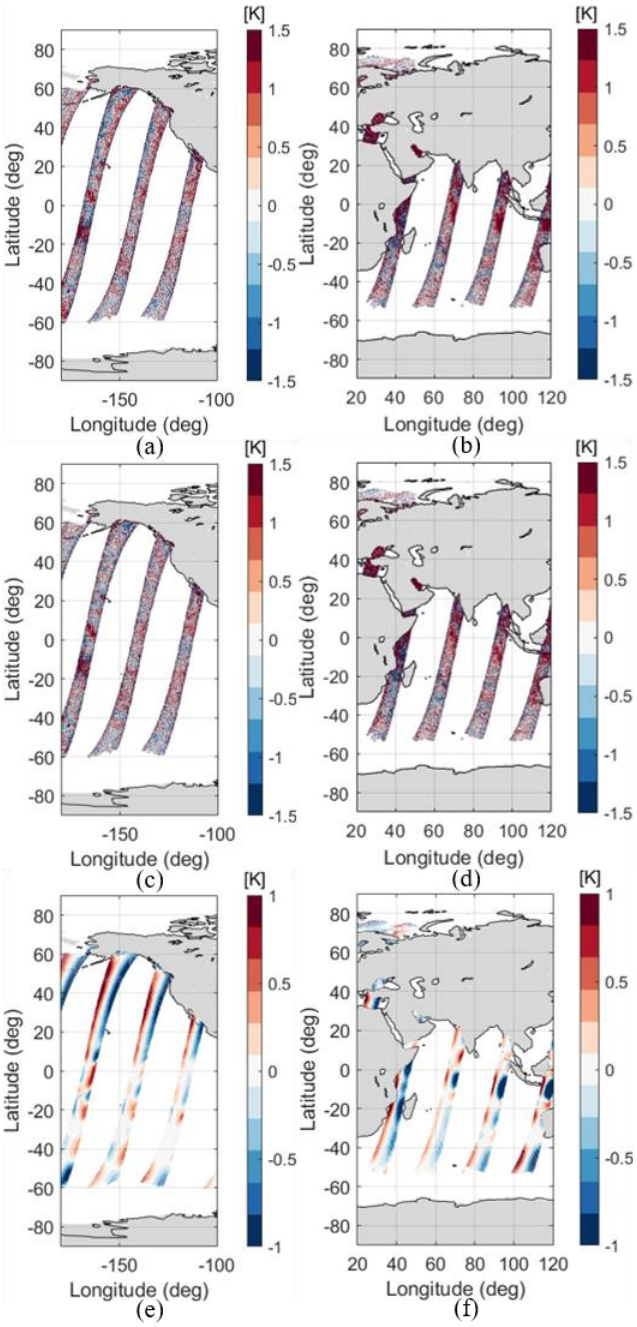

Fig. 10. Daily map (descending orbits) of the difference between the measurements (SMOS corrected TB) and modeled TB for the X-polarization. Top: using L1 VTEC, middle: using SMOS-derived VTEC, bottom: difference between top plots and middle ones.

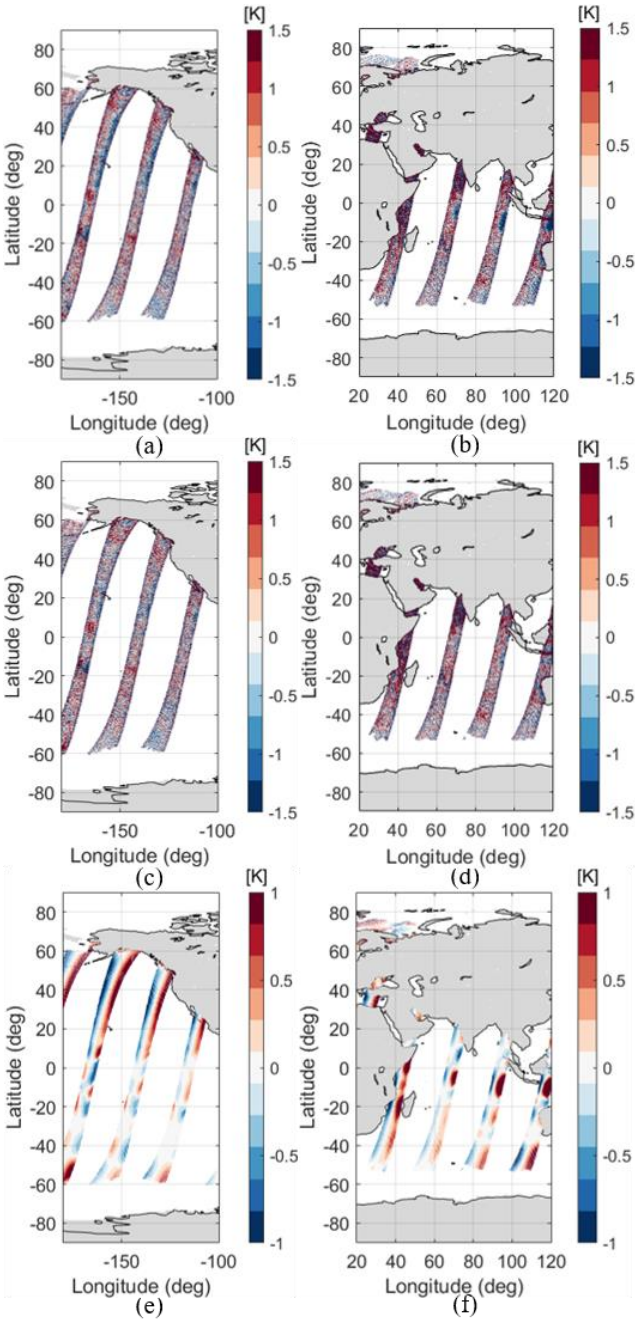

Fig. 11. Daily map (descending orbits) of the difference between the measurements (SMOS corrected TB) and modeled TB for the Y-polarization. Top: using L1 VTEC, middle: using SMOS-derived VTEC, bottom: difference between top plots and middle ones.

Systematic errors found when the L1 VTEC is used (map in the top panel of Fig. 10) are largely mitigated when using the SMOS-derived VTEC maps (map in the middle panel of Fig. 10). The difference between using SMOS-derived VTEC maps and L1 VTEC maps to correct the FRA is shown in the bottom maps of Fig. 10. The impact is particularly evidenced in the Northern hemisphere.

Also, errors are significantly reduced in the Southern Hemisphere, around latitudes of 20ºS (where there is the pool of high TEC), which is especially visible in the Indian Ocean. Similar results have been obtained for the Y-polarization (Fig. 11).

VI. Conclusion

In this work, the error contribution to the FRA estimated from SMOS measurements has shown to be temporal stable. By correcting this contribution, the systematic errors found in the SMOS-derived VTEC maps by using the methodology defined in [1] have been largely mitigated (Fig. 5).

In terms of TB stability, significant improvements are observed in descending orbits. Overall, biases in all the polarizations are reduced when using SMOS-derived VTEC instead of the L1 VTEC. Main improvements are located in the

Southern Hemisphere. The gradient of T3 bias when using L1 VTEC is mostly mitigated when using SMOS VTEC maps. For ascending orbits, the impact on TB in X and Y-polarizations is very low, since the VTEC varies much less than in descending orbits. For the third Stokes parameter, biases are much more stable along the orbits.

The impact of using the SMOS-derived VTEC maps on the spatial biases instead of the L1 VTEC is also positive. The part of the FoV of higher incidence angles improves very significantly in all the polarizations. The overall impact will be quite important in terms of retrieved salinity, since spatial biases are significantly reduced.

Daily maps of the difference between SMOS TB and modeled TB are also improved when using SMOS-derived VTEC maps, showing a clear reduction of systematic patterns, more evident in the Northern Hemisphere.

The assessment of the impact of these SMOS VTEC maps on the TB quality has been focused over the ocean, where the impact of ionospheric corrections is stronger. However, the VTEC maps can be derived from SMOS radiometric data independently of the target seen by the instrument, even though over land it is more challenging. Main limitations to obtain accurate VTEC retrievals over land are in (i) RFI-contaminated regions, since interferences degrade the quality of the SMOS brightness temperatures and therefore, of the VTEC maps; and (ii) regions where the brightness temperatures in X and Y-polarizations are very similar and the third Stokes parameter tends to 0 K, such as in the case of dense forests. As part of the L1 ESL activities, next steps would be aimed at (i) evaluating the performance of using SMOS-derived VTEC maps over land and (ii) using there SMOS global VTEC maps for correcting the FRA and then retrieve salinity and soil moisture to assess the final impact on the geophysical retrievals.

REFERENCES

[1] R. Rubino *et al.*, "Deriving VTEC Maps from SMOS Radiometric Data," *Remote Sens.*, vol. 12, no. 10, p. 1604, May 2020, doi: 10.3390/rs12101604.

[2] D. M. Le Vine and S. Abraham, "The effect of the ionosphere on remote sensing of sea surface salinity from space: absorption and emission at L band," *IEEE Trans. Geosci. Remote Sens.*, vol. 40, no. 4, pp. 771–782, Apr. 2002, doi: 10.1109/TGRS.2002.1006342.

[3] S. H. Yueh, "Estimates of Faraday rotation with passive microwave polarimetry for microwave remote sensing of Earth surfaces," *IEEE Trans. Geosci. Remote Sens.*, vol. 38, no. 5, pp. 2434–2438, Sep. 2000, doi: 10.1109/36.868900.

[4] P. Alken, S. Maus, A. Chulliat, and C. Manoj, "NOAA/NGDC candidate models for the 12th Generation International Geomagnetic Reference Field," *Earth Planets Space 2015*, vol. 67, 2015, doi: 10.1186/s40623-015-0215-1.

[5] J. Barbosa, "SMOS Level 1 and Auxiliary Data Products Specifications," Indra Sistemas, SO-TN-IDR-GS-0005, Aug. 2014.

[6] I. Corbella, W. Lin, F. Torres, N. Duffo, and M. Martin-Neira, "Faraday Rotation Retrieval Using SMOS Radiometric Data," *IEEE Geosci. Remote Sens. Lett.*, vol. 12, no. 3, pp. 458–461, Mar. 2015, doi: 10.1109/LGRS.2014.2345845.

[7] "Daily and monthly sunspot number (last 13 years) | SILSO." http://www.sidc.be/silso/dayssnplot (accessed Mar. 13, 2019).

[8] S. Guimbard, J. Gourrion, M. Portabella, A. Turiel, C. Gabarro, and J. Font, "SMOS Semi-Empirical Ocean Forward Model Adjustment," *IEEE Trans. Geosci. Remote Sens.*, vol. 50, no. 5, pp. 1676–1687, May 2012, doi: 10.1109/TGRS.2012.2188410.

[9] S. Zine *et al.*, "Overview of the SMOS Sea Surface Salinity Prototype Processor," *IEEE Trans. Geosci. Remote Sens.*, vol. 46, no. 3, pp. 621–645, Mar. 2008, doi: 10.1109/TGRS.2008.915543.

[10] J. Tenerelli and N. Reul, "Analysis of L1PP calibration approach impacts in SMOS TB and 3-days SSS retrievals over the Pacific using an alternative Ocean Target Transformation applied to L1OP data," 2010.

[11] R. Oliva, "SMOS ESLs 2020+ Technical Note on the T3 latitudinal gradient across-task T3." Zenithal Blue Technologies, Jun. 2020.

[12] J.-L. Vergely, P. Waldteufel, J. Boutin, X. Yin, P. Spurgeon, and S. Delwart, "New total electron content retrieval improves SMOS sea surface salinity," *J. Geophys. Res. Oceans*, vol. 119, no. 10, pp. 7295–7307, Oct. 2014, doi: 10.1002/2014JC010150.